

Novel stripe-type charge ordering in the metallic A-type antiferromagnet $\text{Pr}_{0.5}\text{Sr}_{0.5}\text{MnO}_3$

R. Kajimoto,¹ H. Yoshizawa,² Y. Tomioka,³ and Y. Tokura^{3,4}

¹Department of Physics, Ochanomizu University, Bunkyo-ku, Tokyo 112-8610, Japan

²Neutron Scattering Laboratory, Institute for Solid State Physics,
University of Tokyo, Tokai, Ibaraki 319-1106, Japan

³Joint Research Center for Atom Technology (JRCAT), Tsukuba, Ibaraki 305-8562, Japan

⁴Department of Applied Physics, University of Tokyo, Bunkyo-ku, Tokyo 113-8656, Japan

(Dated: December 2, 2024)

We demonstrate that an A-type antiferromagnetic (AFM) state of $\text{Pr}_{0.5}\text{Sr}_{0.5}\text{MnO}_3$ exhibits a novel charge ordering which governs the transport property. This charge ordering is stripe-like, being characterized by a wave vector $\mathbf{q} \sim (0, 0, 0.3)$ with very anisotropic correlation parallel and perpendicular to the stripe direction. This charge ordering is specific to the manganites with relatively wide one-electron band width (W) which often exhibit a *metallic* A-type AFM state, and should be strictly distinguished from the CE-type checkerboard-like charge ordering which is commonly observed in manganites with narrower W such as $\text{La}_{1-x}\text{Ca}_x\text{MnO}_3$ and $\text{Pr}_{1-x}\text{Ca}_x\text{MnO}_3$.

PACS numbers: 71.27.+a, 71.30.+h, 71.45.Lr, 75.30.Vn

Perovskite manganites have attracted enormous interests because they exhibit a colossal magnetoresistance (CMR) effect with hole doping, where the conductivity shows a significant increase when a ferromagnetic (FM) state is induced [1]. For the most intensively studied CMR systems $\text{Pr}_{1-x}\text{Ca}_x\text{MnO}_3$ and $\text{La}_{1-x}\text{Ca}_x\text{MnO}_3$, a consensus seems to be reached concerning the mechanism of CMR. In these systems, a so-called ‘‘CE-type’’ charge ordering which appears at $x \sim 1/2$ is considered to be an essential ingredient. In the paramagnetic state of lightly doped manganites, the CE-type charge ordering causes insulating behavior of the resistivity. The reduction of the charge-ordered region with lowering temperature (T) or application of magnetic fields leads to a percolative growth of the FM metallic region, and finally induces an insulator-to-metal transition [2].

One of the important features of these compounds is that these materials have a relatively narrow one-electron band width (W), and exhibits a wide region of the CE-type charge ordered state on their hole-concentration versus T phase diagrams [3]. On the other hand, the CMR phenomenon is not limited to the narrow W manganites, and is indeed observed in systems with wider W such as $\text{Pr}_{0.5}\text{Sr}_{0.5}\text{MnO}_3$ [5], $\text{Nd}_{1-x}\text{Sr}_x\text{MnO}_3$ with $x \gtrsim 1/2$ [6], and $\text{La}_{2-2x}\text{Sr}_{1+2x}\text{Mn}_2\text{O}_7$ with $x = 0.4$ [7]. An important characteristics of these compounds is that all of them show a *highly conductive* A-type antiferromagnetic (AFM) state, and some of them even lack the CE-type charge ordering. The variation of the phase diagram as a function of W is schematically depicted in Fig. 1. In contrast to a manganite with a narrow W (indicated by a thin dashed line), a manganite with a relatively wider W (a thick dashed line) generally shows a following sequence of spin/charge ordering upon hole doping: insulating A-type AFM \rightarrow metallic FM \rightarrow *metallic* A-type AFM \rightarrow insulating C-type, and finally insulating G-type

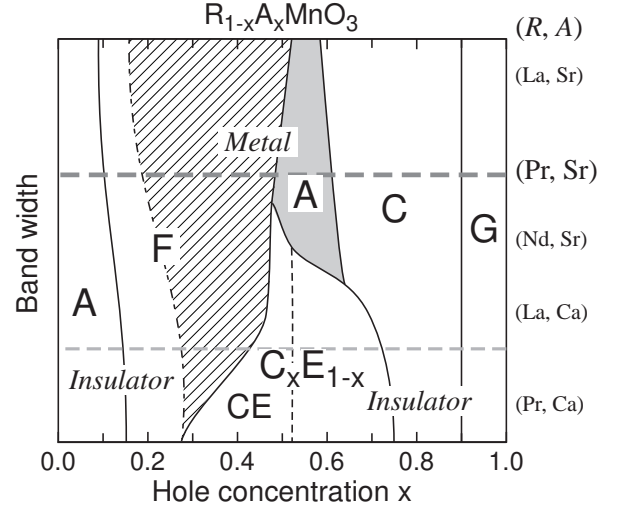


FIG. 1: Schematic phase diagram of $R_{1-x}A_x\text{MnO}_3$. F denotes FM state. A, CE, C, and G denote A-type, CE-type, C-type, and G-type AFM states, respectively. C_xE_{1-x} represents incommensurate charge/orbital ordered state [3].

AFM states. Clearly, the most important feature here is a lack of the CE-type spin/charge ordering and the appearance of the *metallic* A-type AFM [8, 9]. In the metallic A-type AFM, a planar orbital-ordered state with $d(x^2 - y^2)$ orbitals is established around $x = 1/2$ [6, 10]. This orbital ordering mediates the FM coupling within the orbital-ordered planes in which doped carriers possess a fairly large mobility [6, 11]. At the same time, the $d(x^2 - y^2)$ -type orbital ordering favors the AFM coupling perpendicular to the orbital-ordered planes, and results in an overall A-type AFM spin state. The scenario for the CMR phenomenon based on the CE-type charge ordering is clearly irrelevant in this case, and another microscopic mechanism ought to be invoked.

To unravel this issue, we chose one of the cubic A-type AFM manganites, $\text{Pr}_{0.5}\text{Sr}_{0.5}\text{MnO}_3$, and performed a detailed neutron diffraction study. $\text{Pr}_{0.5}\text{Sr}_{0.5}\text{MnO}_3$ exhibits a first-order phase transition from a FM metal to an AFM less-conductive state at $T_N \sim 140$ K, accompanied with a structural transition as shown in Fig. 3(a) [5]. It exhibits a significant MR ($> 90\%$) below T_N . With a high quality single crystal sample, we found that there exists a novel stripe-type charge ordering with the modulation vector $q \sim 0.3$ r.l.u. (reduced lattice units) at all T . In what follows, we shall demonstrate that the quasi-stripe order is intrinsic to the planar $d(x^2 - y^2)$ -type orbital ordering, and the transport property in the *metallic* A-type AFM is, in fact, controlled by the interplay between the stripe-type charge ordering and the double-exchange (DE) interactions. The present results provide strong evidence that the physics of the CMR phenomena in the A-type AFM manganites is fundamentally different from the phase separation scenario based on the CE-type charge ordering in the narrow W manganites.

The single crystal sample well-characterized in the preceding studies [5, 11, 12] was reinvestigated by neutron diffraction technique. An incident neutron momentum $k_i = 3.83 \text{ \AA}^{-1}$ and a combination of $40'-40'-80'$ collimators were utilized at the triple axis spectrometer GP-TAS installed at the JRR-3M reactor in JAERI, Tokai, Japan. Two pyrolytic graphite filters were placed before and after the sample to suppress higher-order contaminations. The sample was mounted in an Al can filled with He gas, and was attached to the cold head of a closed-cycle helium gas refrigerator. The temperature was controlled within an accuracy of 0.2 K.

The crystal structure of $\text{Pr}_{0.5}\text{Sr}_{0.5}\text{MnO}_3$ is tetragonal $I4/mcm$ with $a = b \sim 5.4 \text{ \AA}$ and $c/\sqrt{2} \sim 5.5 \text{ \AA}$ in the paramagnetic (PM) and FM states and monoclinic $P2_1/n$ with $a \sim c \sim 5.4 \text{ \AA}$, $b/\sqrt{2} \sim 5.5 \text{ \AA}$, and $\beta \sim 91^\circ$ in the AFM state [11, 13]. For simplicity, we employ the cubic notation with $a \sim 3.8 \text{ \AA}$ so that the FM layers of the A-type AFM structure are perpendicular to the $[010]$ direction. All the diffraction measurements were carried out on the $(h, 0, l)$ scattering plane to measure the correlations within the FM layers in the A-type AFM states.

To examine whether $\text{Pr}_{0.5}\text{Sr}_{0.5}\text{MnO}_3$ exhibits a charge ordering, we surveyed the $(h, 0, l)$ scattering plane at selected T s. Figure 2 presents a map of the scattering intensities collected around $(0, 0, 2)$ in the A-type AFM phase at $T = 7$ K, in the FM phase at 180 K, and in the PM phase at 275 K, respectively. The intense fundamental nuclear Bragg reflection was observed at $(0, 0, 2)$. At 7 K, A-type AFM Bragg reflections are observed at $(\pm 0.5, 0, 2)$. Two ring-shaped scatterings observed at all T s are powder scattering from the Al sample cell. In addition, twinning and mosaic distributions of the crystal yield a nuclear reflection near $(-0.1, 0, 2)$ as well as an A-type AFM Bragg reflection near $(0, 0, 1.6)$, but they were slightly displaced from the commensurate positions

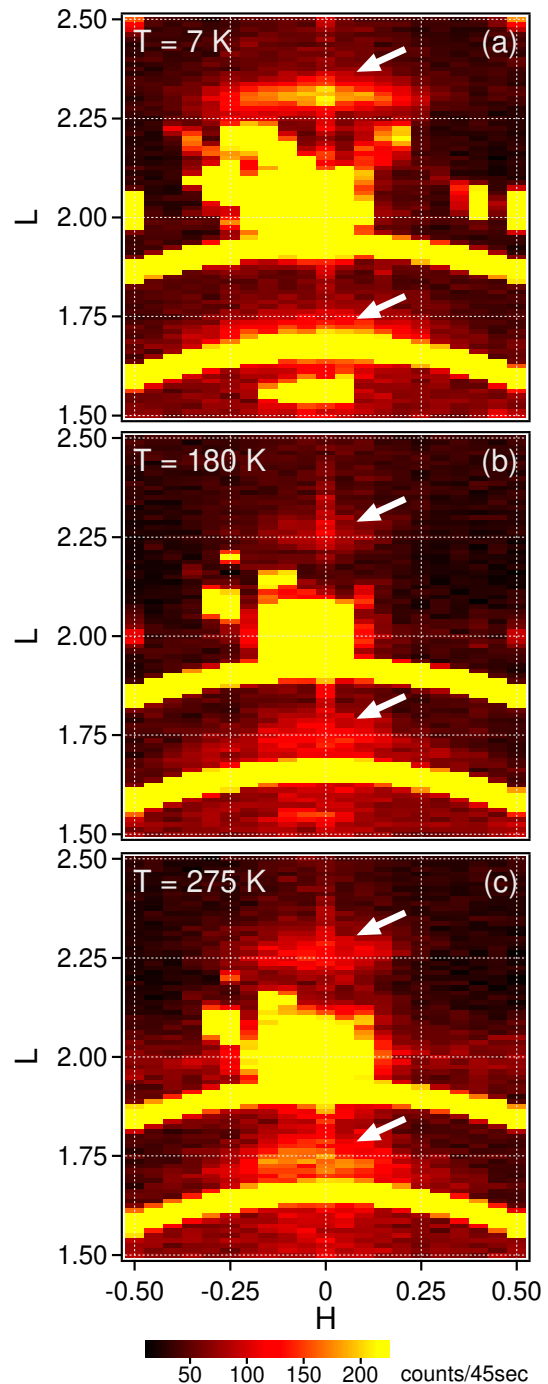


FIG. 2: Intensity maps around $(0, 0, 2)$ at (a) $T = 7$ K, (b) 180 K, and (c) 275 K. Two ring-shaped scatterings observed at all temperatures are due to the Al sample cell. At 7 K, A-type AFM Bragg reflections are observed at $(\pm 0.5, 0, 2)$ in addition to the fundamental Bragg reflection at $(0, 0, 2)$.

due to the small deviations of the lattice constants of respective domains from the ideal cubic symmetry. We also observed the weak CE-type superlattice reflections appearing at $Q \sim (\pm 0.2, 0, 2.2)$ in the AFM phase [Fig. 2(a)]. In the present case, however, the CE-type ordered

region has practically no influence on the transport property, because its volume fraction is negligibly small, being consistent with the lack of the CE-type AFM reflections in the previous powder neutron diffraction study [11]. We note that the coexistence of the A-type metallic AFM region and the parasitic CE-type insulating region was frequently observed in the manganites with $x \sim 1/2$ [10, 14, 15].

The important new results in Fig. 2 are anisotropic diffuse scatterings indicated by white arrows. They are centered at $\mathbf{Q} \sim (0, 0, 2 \pm 0.3)$, and are elongated towards the [100] direction. The anisotropy of their profiles indicates that the correlation length along \mathbf{Q} is much longer than that perpendicular to \mathbf{Q} . Although the diffuse scattering becomes weaker in the FM and PM states, it remains finite, but the position of the signal shifts slightly towards $\mathbf{Q} \sim (0, 0, 2 \pm 0.25)$. Because the similar scatterings are observed at large Q but less clear at small Q , the origin of the scatterings is attributable to lattice modulations. Due to the twinning domains with propagation vectors $\mathbf{q} = (0, 0, 0.3)$ or $(0.3, 0, 0)$, the similar scattering is expected at $(\pm 0.3, 0, 2)$ in Fig. 2(a), but we found no signal at corresponding positions. This suggests that the lattice modulations consist of a longitudinal component, because the scattering cross section has a term $|\mathbf{Q} \cdot \boldsymbol{\eta}|^2$ where $\boldsymbol{\eta}$ represents a displacement vector of constituent ions. A similar feature was also observed in the stripe-like charge ordering in a two-dimensional (2D) A-type AFM manganite $\text{La}_{2-2x}\text{Sr}_{1+2x}\text{Mn}_2\text{O}_7$ [16, 17].

In order to confirm that the newly found diffuse scattering is originated from the charge ordering, its influence on the transport property was examined by the T dependences of the intensity, the peak width, and the wave vector of the diffuse scattering. We found a strong correlation between the resistivity and these quantities, which establishes that the observed diffuse scattering indeed arises from the charge ordering. In Figs. 3(a) and (b) are plotted the T dependence of the resistivity and that of the diffuse intensity at $(0, 0, 2.3)$, respectively [18]. Fig. 3(c) shows the T dependence of the peak position (the modulation wave vector) and the peak width (FWHM) measured along the longitudinal direction (perpendicular to the stripes). In the A-type AFM state for $T < T_N$, the correlation of the charge ordering is well-developed. The diffuse peak has large intensity, and its width is quite sharp, although it is much broader than the instrumental resolution (~ 0.03 r.l.u.). In this phase, the resistivity exhibits a steep increase with lowering T . At T_N , the system undergoes the first order transition. The intensity of the charge ordering and the resistivity show sudden decreases at T_N . In addition, the correlation length of the charge ordering decreases, while its peak position shifts to a smaller wave vector on crossing T_N . Upon raising T , however, the intensity of the charge ordering gradually increases, and the resistivity recovers the metallic behavior. Around T_C , the resistivity as well as the intensity

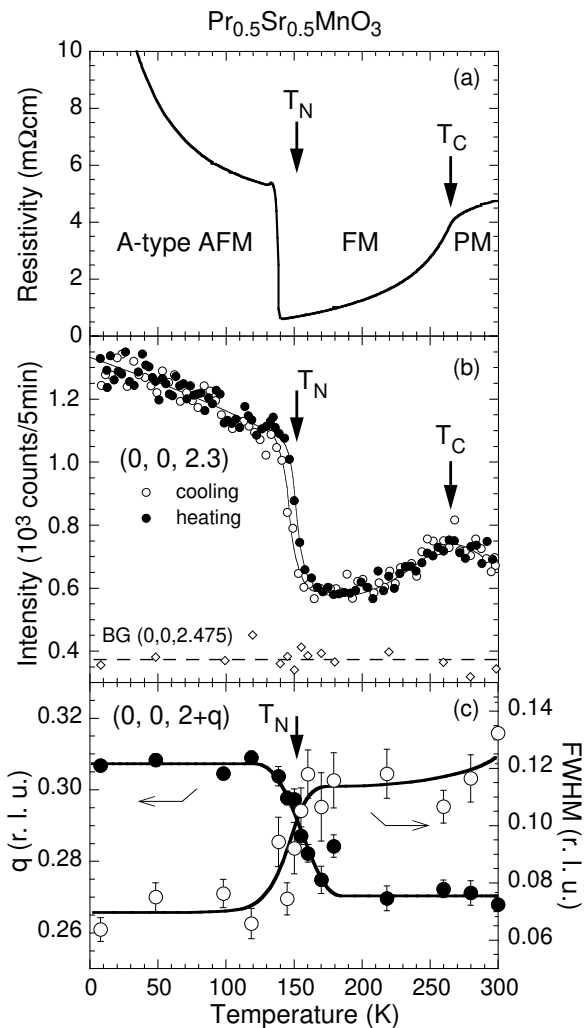


FIG. 3: (a) Temperature dependence of the resistivity. (b) Temperature dependence of the intensity at $(0, 0, 2.3)$. The background (BG) intensity measured at $(0, 0, 2.475)$ is also shown. Open symbols and closed symbols denote the data for cooling and for heating, respectively. (c) Temperature dependence of the wave vector (closed symbols) and the peak width (FWHM) (open symbols) of the charge order peak $(0, 0, 2.3)$.

of the charge ordering shows a cusp and enters the PM state. Note that the novel diffuse scattering subsists in the FM as well as PM states in $\text{Pr}_{0.5}\text{Sr}_{0.5}\text{MnO}_3$.

These results clearly indicate that the newly-discovered charge ordering is intrinsic to the A-type AFM $\text{Pr}_{0.5}\text{Sr}_{0.5}\text{MnO}_3$ with $d(x^2 - y^2)$ orbital ordering. In particular, the transport property of $\text{Pr}_{0.5}\text{Sr}_{0.5}\text{MnO}_3$ is controlled by the interplay between the DE interactions and the novel charge ordering which is embedded in the MnO_2 planes with the $d(x^2 - y^2)$ orbital ordering. Since a similar charge ordering was observed in the 2D A-type AFM manganites, the existence of such charge ordering must be independent to the spatial dimensionality of the manganites, and is one of the key features of the wide W manganites which are accompanied with the $d(x^2 - y^2)$ -

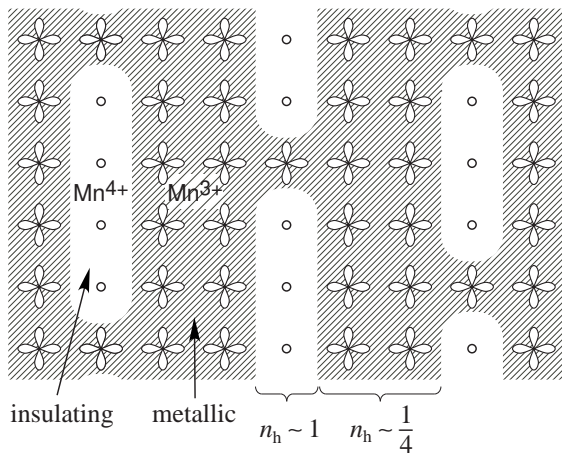


FIG. 4: Schematic illustration of the charge order and orbital order with $q = 1/3$ r.l.u. Cloverleaf symbols represent the $d(x^2 - y^2)$ orbitals. n_h denotes the hole concentration within the Mn^{4+} stripe or the Mn^{3+} -like matrix.

type orbital ordering.

We propose that the simplest model of the charge ordering which is compatible with these observations may be a stripe-like object drawn in Fig. 4. In this model, Mn^{4+} ions segregate within the metallic matrix of Mn^{3+} -like sites with $d(x^2 - y^2)$ orbitals, and form stripe-like objects along the Mn-O-Mn bond direction. The Mn^{4+} stripes are insulating, and they block the hopping of the e_g electrons, while the Mn^{3+} -like matrix is metallic. Thus, the conductivity of the A-type AFM system is controlled by the number of stripe-like objects within the $d(x^2 - y^2)$ -type orbital-ordered matrices. In this sense, it is distinctly different from the percolative picture of the CMR phenomenon for the narrow W manganites, in which a phase separation between the CE-type charge ordered regions and the FM metallic regions is essential for the origin of the CMR behavior.

The observed stripe-like ordering has some distinct features. First of all, the amplitude of the wave vector $q \sim 0.3$ r.l.u. is far apart from its nominal hole concentration $x = 1/2$. For the model with $q = 1/3$ r.l.u. depicted in Fig. 4, the hole concentration of the Mn^{4+} stripe is fixed to 1, while that of two Mn^{3+} lines be $1/4$, resulting in the overall concentration $x = 1/2$. The large discrepancy between the hole concentration and the amplitude of the wave vector is also observed in 2D manganites $\text{La}_{2-2x}\text{Sr}_{1+2x}\text{Mn}_2\text{O}_7$ where the wave vector is effectively fixed at $q \sim 1/3$ for a wide region of the hole concentration [16]. It should be noted, however, that the wave vector of the stripe-like diffuse scattering in $\text{Pr}_{0.5}\text{Sr}_{0.5}\text{MnO}_3$ is slightly shifted through the transition from the A-type AFM state to the FM state as seen in Fig. 3(c). This behavior indicates that the mechanism of the formation of the stripe-type charge ordering in wide W manganites is susceptible to the change of the spin structure and

concomitant change of the electronic state.

An effectively fixed wave vector at $q \sim 1/3$ suggests that the relative distance between such stripes remains almost the same for a wide region of the hole concentration by tuning the hole concentrations within stripes and the Mn^{3+} -like matrix regions. This interpretation is consistent with the observed strong anisotropy of the diffuse scattering. The striking asymmetry of the profiles of the diffuse scattering was observed as shown in Fig. 2. The correlation length ξ_{\parallel} parallel to the stripe is much shorter than ξ_{\perp} perpendicular to the stripe. From the width of the profile along the [100] direction, ξ_{\parallel} is estimated to be $4a \sim 5a$. These results are consistently explained by the proposed stripe picture. In particular, e_g electrons enter every 4 ~ 5 sites of the line of Mn^{4+} ions as depicted in Fig. 4. The tuning of the hole concentration causes the deviation of the hole density within stripes to be $1 - \delta$, while that of the Mn^{3+} -like matrix regions $1/4 + \delta/2$, respectively. For a finite δ , some excess electrons intervene Mn^{4+} stripes, while some holes are accommodated within the Mn^{3+} -like $d(x^2 - y^2)$ -type orbital-ordered matrix. Consequently, the stripe ordering consist of a number of short segments as shown in Fig. 4.

One more important feature of the present stripe-like charge ordering is that the charge stripes are parallel to the Mn-O bonds in contrast to the CE- and C_xE_{1-x} -type charge ordering [19]. The direction of the stripes can be explained by the large mobility within the orbital-ordered planes. The DE mechanism mediated by the hopping of holes is a dominant interaction within the metallic orbital-ordered planes, while the superexchange (SE) interactions are dominant within stripes and at the boundaries between Mn^{4+} stripes and metallic regions. In the case of the “parallel” charge order, the number of the Mn-O-Mn bonds mediating the DE interactions is much larger than that in the case of the “diagonal” charge order. When W is sufficiently large, the DE interaction overwhelms the SE interaction, and the parallel charge order is favored by maximizing the number of the DE interactions. On the contrary, when W is small, the SE interactions dominate, and favor the diagonal charge order known as the CE- and C_xE_{1-x} -type [20]. We would like to point out that a similar relation between the charge mobility and the direction of stripes holds in the well-known stripe ordered systems, *i.e.* high- T_c cuprates [21] and isomorphous nickelates [22]. In the metallic cuprates, the stripes are “parallel”, while they are “diagonal” in the insulating nickelates. Note that the $d(x^2 - y^2)$ orbital state is also common to both A-type AFM manganites and high- T_c cuprates: the stripes in both *metallic* materials are formed in the matrix of $d(x^2 - y^2)$ orbital states.

To summarize, a neutron diffraction study was performed on a single crystal of $\text{Pr}_{0.5}\text{Sr}_{0.5}\text{MnO}_3$. We found a very anisotropic charge ordering with wave vector $\mathbf{q} \sim (0, 0, 0.3)$. The diffuse scattering is consistent with

the stripe-like charge ordering. This novel charge ordering exists in the manganites with a wide one-electron band width and with the $d(x^2 - y^2)$ -type orbital ordering regardless of its spatial dimensionality. The transport property is controlled through the competition between the novel stripe-like charge ordering and the DE interactions. The CMR phenomenon in these materials must be understood on the basis of this “*stripe-like charge ordering*”.

We thank H. Kawano-Furukawa for valuable discussions. This work was supported by a Grand-In-Aid for Scientific Research from the Ministry of Education, Culture, Sports, Science, and Technology, Japan and by the New Energy and Industrial Technology Development Organization (NEDO) of Japan.

-
- [1] M. Imada, A. Fujimori, and Y. Tokura, *Rev. Mod. Phys.* **70**, 1039 (1998).
- [2] M. Uehara, S. Mori, C. H. Chen, and S.-W. Cheong, *Nature (London)* **399**, 560 (1999).
- [3] The incommensurate charge and orbital order observed at $x > 1/2$ [19] can be regarded as an extension of the CE-type charge/orbital order, and we represent it by $C_x E_{1-x}$ in Fig. 1 following Ref. [4].
- [4] E. Dagotto, T. Hotta, and A. Moreo, *Phys. Rep.* **344**, 1 (2001).
- [5] Y. Tomioka, A. Asamitsu, Y. Moritomo, H. Kuwahara, and Y. Tokura, *Phys. Rev. Lett.* **74**, 5108 (1995).
- [6] H. Kuwahara, T. Okuda, Y. Tomioka, A. Asamitsu, and Y. Tokura, *Phys. Rev. Lett.* **82**, 4316 (1999).
- [7] Y. Moritomo, A. Asamitsu, H. Kuwahara, and Y. Tokura, *Nature (London)* **380**, 141 (1996).
- [8] Y. Moritomo, H. Kuwahara, Y. Tomioka, and Y. Tokura, *Phys. Rev. B* **55**, 7549 (1997).
- [9] T. Akimoto, Y. Maruyama, Y. Moritomo, A. Nakamura, K. Hirota, K. Ohoyama, and M. Ohashi, *Phys. Rev. B* **57**, R5594 (1998).
- [10] R. Kajimoto, H. Yoshizawa, H. Kawano, H. Kuwahara, Y. Tokura, K. Ohoyama, and M. Ohashi, *Phys. Rev. B* **60**, 9506 (1999).
- [11] H. Kawano, R. Kajimoto, H. Yoshizawa, Y. Tomioka, H. Kuwahara, and Y. Tokura, *Phys. Rev. Lett.* **78**, 4253 (1997).
- [12] H. Kawano, R. Kajimoto, H. Yoshizawa, Y. Tomioka, H. Kuwahara, and Y. Tokura, *cond-mat/9808286*; H. Yoshizawa, R. Kajimoto, H. Kawano, J. A. Fernandez-Baca, Y. Tomioka, H. Kuwahara, and Y. Tokura, *Mater. Sci. and Eng. B* **63**, 125 (1999); R. Kajimoto, H. Yoshizawa, H. Kawano-Furukawa, H. Kuwahara, Y. Tomioka, and Y. Tokura, *J. Magn. Magn. Mater.* **226-230**, 892 (2001).
- [13] A. Llobet, J. L. García-Muñoz, C. Frontera, and C. Ritter, *Phys. Rev. B* **60**, R9889 (1999).
- [14] Y. Moritomo, T. Akimoto, A. Nakamura, K. Ohoyama, and M. Ohashi, *Phys. Rev. B* **58**, 5544 (1998).
- [15] M. Kubota, H. Yoshizawa, Y. Moritomo, H. Fujioka, K. Hirota, and Y. Endoh, *J. Phys. Soc. Jpn.* **68**, 2202 (1999).
- [16] M. Kubota, Y. Oohara, H. Yoshizawa, H. Fujioka, K. Shimizu, K. Hirota, Y. Moritomo, and Y. Endoh, *J. Phys. Soc. Jpn.* **69**, 1986 (2000).
- [17] L. Vasiliu-Doloc, S. Rosenkranz, R. Osborn, S. K. Sinha, J. W. Lynn, J. Mesot, O. H. Seeck, G. Preosti, A.J. Fedro, and J. F. Mitchell, *Phys. Rev. Lett.* **83**, 4393 (1999).
- [18] The resistivity data in Fig. 3 was measured for another sample. A small discrepancy between the transition temperatures corresponding to T_N in Fig. 3(a) and Fig. 3(b) may be due to the sample dependency.
- [19] S. Mori, Ch. H. Chen, and S-W. Cheong, *Nature (London)* **392**, 473 (1998); P.G. Radaelli, D.E. Cox, L. Capogna, S.-W. Cheong, and M. Marezio, *Phys. Rev. B* **59**, 14440 (1999).
- [20] For a related discussion, see T. Mizokawa and A. Fujimori, *Phys. Rev. Lett.* **80**, 1320 (1998).
- [21] J. M. Tranquada, B. J. Sternlieb, J. D. Axe, Y. Nakamura, and S. Uchida, *Nature (London)* **375**, 561 (1995).
- [22] P. Wochner, J. M. Tranquada, D. J. Buttrey, and V. Sachan, *Phys. Rev. B* **57**, 1066 (1998).